

## Photophysical, hemocompatibility, and anticancer effect of ZnO/MnPcCl NPs: In vitro and in vivo assessments for PDT

S. A. Al-Ghamdi<sup>a</sup>, M. A. Elblbesy<sup>b,c,\*</sup>, S. Khasim<sup>a</sup>, A. A. A. Drawish<sup>a,d</sup>, A. Pasha<sup>e</sup>, T. A. Hamdalla<sup>a,f</sup>, M. E. Moustafa<sup>b</sup>

<sup>a</sup>Department of Physics, Faculty of Science, University of Tabuk, Tabuk, Saudi Arabia

<sup>b</sup>Department of Medical Biophysics, Medical Research Institute, Alexandria University, Egypt

<sup>c</sup>Department of Medical Laboratory Technology, Faculty of Applied Medical Science, University of Tabuk, Saudi Arabia

<sup>d</sup>Department of Physics, Faculty of Education at Al-Mahweet, Sana'a University, Al-Mahweet, Yemen

<sup>e</sup>Department of Physics, Ghousia College of Engineering, Ramanagaram, Karnataka, 562 159, India

<sup>f</sup>Department of Physics, Faculty of Science, Alexandria University, Alexandria, Egypt

Photodynamic therapy (PDT) is an approved promising new treatment modality for a variety of cancers. In combination with nanotechnology, PDT offers the lowest rates of side effects and reveals high treatment efficiency. This study aimed to design and develop a new formulation based on zinc oxide containing Manganese (III) Phthalocyanine Chloride (ZnO/MnPcCl NPs) for use in the PDT protocol and investigate its hemocompatibility with human blood. Additionally, the antitumor activity in mice using the Ehrlich solid tumor as an experimental model was examined. They were non-hemolytic and had no harmful effects on partial thromboplastin time and prothrombin time. ZnO/MnPcCl NPs in conjunction with laser (670 nm/0.6 j/cm<sup>2</sup>) had significantly better in vivo anticancer efficacy compared with pristine ZnO/MnPcCl NPs and laser. These findings confirm that ZnO/MnPcCl NPs could serve as an efficient and biocompatible PDT system for anticancer. Also, this study confirms that the combination between PDT and nanotechnology can improve the shortcomings of photodynamic therapy.

(Received December 30, 2021; Accepted March 9, 2022)

**Keywords:** Phthalocyanine, Zinc oxide, Nanoparticles, Hemocompatibility, Anticancer activity

### 1. Introduction

Photodynamic therapy (PDT) is fast becoming an essential therapeutic tool in many diseases with a minimally invasive procedure. As a cancer-treatment method, PDT has a series of advantages over other methods such as surgery, chemotherapy, and radiotherapy [1, 2]. The action mechanism of PDT is depended on the production of oxidative species by a photosensitizer (PS). Oxidative stress has the potential to induce cell death or a therapeutically significant stress response. The anticancer mechanisms of PDT include necrosis, apoptosis, or autophagy [3].

PSs are molecules that absorb light often in the visible or infrared spectrum and converting it to chemical potential [4]. The first generation of PS, Photofrin, consisted of complex mixtures of porphyrinoids that were exhibited promising anticancer PDT results [5]. The second and third generations of PS include phthalocyanines (Pcs), benzoporphins, purpurins, chlorins, porphycenes, pheophorbides, bacteriochlorins, and bacteriopheophorbides molecules showed improved photodynamic activity and chemical purity compared to first-generation PS [6-10].

Phthalocyanines (Pcs) have been identified as a successful artificial dye and PS. They are characterized by high thermal and chemical stability [11-14]. Many Pcs derivatives have become

---

\* Corresponding author: mohamed.elblbisy@alexu.edu.eg  
<https://doi.org/10.15251/DJNB.2022.171.323>

available, and their physical and chemical properties have been studied extensively [15]. Pcs and their derivatives are increasingly recognized in many applications such as dyes and pigments, solar cells, optical storage medium, and electrocatalyst [16, 17]. Recently, many researchers focused on using Pcs as a photodynamic agent for cancer therapy [14, 18].

Nano drug delivery systems, such as nanoparticles and liposomes, have also been used recently to improve the anti-cancer effect of the second and third generation of PS [19, 20]. Hydrophobic Pc derivatives are recognized as promising candidates for being associated with nanostructured drug delivery systems [21]. Hydrophobic Pcs show excellent accumulation in cancerous cells. The higher hydrophobicity leads to accelerate clearance from the body by mononuclear phagocytes [22]. Several studies have examined nanostructured systems that reduce related drawbacks of Pcs hydrophobicity in aqueous media [23-25]. However, major problems with these systems employ a high level of organic solvents and are not easily scaled up.

The present article describes the synthesis and characterization of Zinc Oxide/Manganese (III) Phthalocyanine chloride nanoparticles (ZnO/MnPcCl NPs). The photophysical and hemocompatibility of the synthetic NPs will be examined. Additionally, Its *in vivo* anticancer efficacy was evaluated in mice bearing Ehrlich ascites carcinoma in association with light (670 nm of 0.6 J/cm<sup>2</sup>).

## 2. Materials and methods

### 2.1. ZnO/MnPcCl NPs Preparation Method

ZnO nanoparticles have been prepared as reported by Beek *et al.* [1] and Weller *et al.* [2] through the hydrolysis and condensation of zinc acetate dihydrate by potassium hydroxide in an alcoholic medium at low-temperature conditions. The ZnO nanoparticles settled at the bottom, and the excess mother liquor was removed and the precipitate was washed with methanol. The precipitate was then dried at 60 °C. The loading Mn-dye onto zinc oxide nanoparticles was done as described by Al-Ajmi *et al.* [3] in which, 10 mg of dried powder was dispersed in 10 ml ethanol, then 10 mg of dye was added with sonication for 30 min to be tapped onto zinc oxide nanoparticles, Centrifugation was used to remove solvents and unreacted materials at 10000 rpm for 10 min to obtain dye loaded ZnO NPs, which were dried at 60 °C overnight. The concentration of untrapped dye was measured by UV-vis spectrophotometer (care series UV-Vis-NIR spectrophotometer, Australia) at 716 nm, which was used to calculate the percent encapsulation efficiency (EE) of ZnO/MnPcCl NPs in ZnO NPs As follows:

$$EE = \frac{\text{Initial Conc.} - \text{free concentration}}{\text{Initial Conc}} \times 100 \quad (1)$$

### 2.2. Scanning electron microscopy

The shape and surface morphology of ZnO and ZnO/ MPC NP were both investigated in a scanning electron microscope (JSM-7001F; JEOL, Tokyo, Japan). Briefly, 20 µL of ZnO and ZnO/ MPC NP dispersed in water were deposited on copper supports. Next, the sample was left to dry for 5 hours at room temperature in a jar containing silica gel desiccant, and then coated with gold using Blazers SCD 050® sputter coater.

### 2.3. Transmission electron microscopy (TEM) Measurements

A high-resolution transmission electron microscope (Joel, JSM-6360 LA-Japan) was used to characterize the size and morphology of ZnO/MnPcCl NPs. An aliquot of the sample (100 µL) was added onto a 200-mesh TEM copper grid. After a 5-min drying time at room temperature, the excess sample was carefully removed by a piece of filter paper. Then the sample was stained using an aliquot of aqueous uranyl acetate solution (2%, w/v).

### 2.4. Fourier-transform infrared (FT-IR) spectroscopy

FT-IR studies were carried out using an FT-IR spectrometer (Vertex70 RAM II, Germany). A dry sample was pressed onto the ATR crystal, and the infrared spectrum was

recorded from 4000 to 400  $\text{cm}^{-1}$  at room temperature and resolution of 4  $\text{cm}^{-1}$ . The studied samples were MnPcCl and ZnO/MnPcCl NPs.

### 2.5. Photophysical properties of ZnO/ MnPcCl NPs

The absorption spectrum of ZnO/MnPcCl NPs was recorded on a Shimadzu UV-VIS 2550 spectrophotometer. UV-VIS spectra of ZnO/ MnPcCl NPs toluene, acetonitrile, and methanol were recorded. An aliquot of 2 mL of toluene, acetonitrile, or methanol was mixed with 0.02 mL of ZnO/MnPcCl NPs solution for determining UV-VIS spectra.

### 2.6. Detection of reactive oxygen species

The probe 1,3-diphenylisobenzofuran (DPBF) was used in the detection of reactive oxygen species (ROS) as described in previous studies [26-28]. Absorption of ZnO/MnPcCl NPs sample of 200  $\mu\text{L}$  was measured at 410 nm and, 25  $^{\circ}\text{C}$ , after mixing with 10  $\mu\text{L}$  of DPBF in ethanol (225  $\mu\text{g}/\text{mL}$ ). Absorption measurement was performed in a transparent 96- well microplate before and immediately after irradiation (670 nm of 0.6  $\text{J}/\text{cm}^2$ ). Optical density at 410 nm before irradiation was considered to be 0% ROS, while the lower plateau absorption values were considered to be 100 % ROS generation. This experiment was performed in triplicate.

### 2.7. In vitro Studies

#### 2.7.1 Hemolysis Test

3ml of human blood samples were incubated with ZnO/MnPcCl NPs for one hour in dark. Other 3 ml were incubated with ZnO/MnPcCl and irradiated with 670 nm. Blood samples after incubation were washed four times by adding to 15 ml of PBS pH 5.7 then centrifuged for 6 min at 3500 rpm. After the final wash, 200  $\mu\text{L}$  of blood were removed from the bottom of the tube and add to 9.8 mL PBS pH 5.7. 100  $\mu\text{L}$  TritonX solutions were prepared at different concentrations from 15  $\text{mg}/\text{mL}$  to .0015  $\text{mg}/\text{mL}$ . 50  $\mu\text{L}$  of blood was added to 100  $\mu\text{L}$  TritonX solutions and incubated at 37 $^{\circ}\text{C}$  for 30 min. After incubation blood samples were centrifuged at 3500 rpm for 6 min and 75  $\mu\text{L}$  of supernatant was collected. Collected supernatants were transferred to 96 well plate and absorbance was measured at 541 nm. A positive control (known lysis) was prepared by adding 50  $\mu\text{L}$  blood solution to 100  $\mu\text{L}$  diH<sub>2</sub>O and freeze -80  $^{\circ}\text{C}$ . the hemolysis percentage was calculated from equation (2).

$$\text{Hemolysis \%} = \frac{OD_{\text{test}} - OD_{\text{-ve}}}{OD_{\text{+ve}} - OD_{\text{-ve}}} \times 100 \quad (2)$$

#### 2.7.2. prothrombin time (PT) assay and Partial thromboplastin time (PTT)

Human blood samples each of 6 mL were decalcified by collecting it into a tube with oxalate. Blood samples were divided into two aliquots. One aliquot was incubated with ZnO/MnPcCl NPs for one hour in dark and the Other was incubated with ZnO/MnPcCl and irradiated with 670 nm. For all blood samples plasma was separated by centrifugation. The PT test was performed by adding the plasma to some source of thromboplastin. The mixture was then incubated in water bath at 37 $^{\circ}\text{C}$  for two minutes. Calcium chloride was added to the mixture and allow clot to form. Prothrombin Time (PT) was taken as the time from the addition of the calcium chloride until the plasma clots. For measuring The Partial thromboplastin time (PTT). The separated plasma was mixed with Calcium and kaolin. The PTT was measured as the time takes for a clot to form, measured in seconds.

### 2.8. In Vivo Studies

The efficiency of PDT was evaluated on mice with Ehrlich tumor. male mice weighing 20-25 g and of age 4-5 weeks were used in this study. The mice were bred in polycarbonate cages under specific pathogen-free conditions. Animals were housed in a room with controlled temperature (23  $\pm$  2  $^{\circ}\text{C}$ ), humidity (55%  $\pm$  7%), and a 12 h light/dark reversed cycle. Induction of Ehrlich's tumor was developed by injection of 0.1 ml ascitic fluid containing 500,000 tumor cells subcutaneously in the thigh of each mouse. The injection by ZnO/MnPcCl NPs was started after the tumor volume reached volume 350-500  $\text{mm}^3$ . The mice were divided randomly into three

groups, each of 20 mice. Group A was Intratumorally injected with 0.2 mL of PBS every 3 days for 15 days and was used as a control. Group B was irradiated on the tumor site with laser (670 nm of  $0.6 \text{ J/cm}^2$ ). Group C was injected with ZnO/MnPcCl NPs in an aqueous solution Intratumorally and irradiated with laser (670 nm of  $0.6 \text{ J/cm}^2$ ) simultaneously. The tumor volume and mouse total body weight were recorded every three days for all groups after the first injection. By the day 15, The tumors were completely removed from mice under anesthesia and weighed. The ellipsoidal tumor volume ( $V$ ) was calculated from Equation (3).

$$V = \frac{\pi}{6} \times D \times d^2 \quad (3)$$

where  $D$  is the tumor dimension at the longest point and  $d$  is the tumor dimension at the widest point.  $D$  and  $d$  were measured with a digital caliper.

### 2.9. Statistical Analysis

All results were expressed as mean  $\pm$  SD of at least three independent measurements. One-way analysis of variance (ANOVA) was used to compare the means among the groups. Statistical significance was defined as  $p < 0.05$ . Data were statistically analyzed using (GraphPad Software Inc., La Jolla, CA, USA).

## 3. Results and discussion

The SEM either for ZnO NP or ZnO/ MnPcCl NP, showed narrow particle size distribution with an average mean size of 20nm and 23 nm for ZnO NP or ZnO/ MnPcCl NP respectively. As can be seen from Figure 1, ZnO NP or ZnO/ MnPcCl NP consist of spherical shaped particles. However, a more agglomerated nature is revealed for ZnO/ MnPcCl NP material, this can be attributed to the added phthalocyanine molecule MnPcCl due to the surface functionalization of ZnO by the MnPcCl molecules[29].

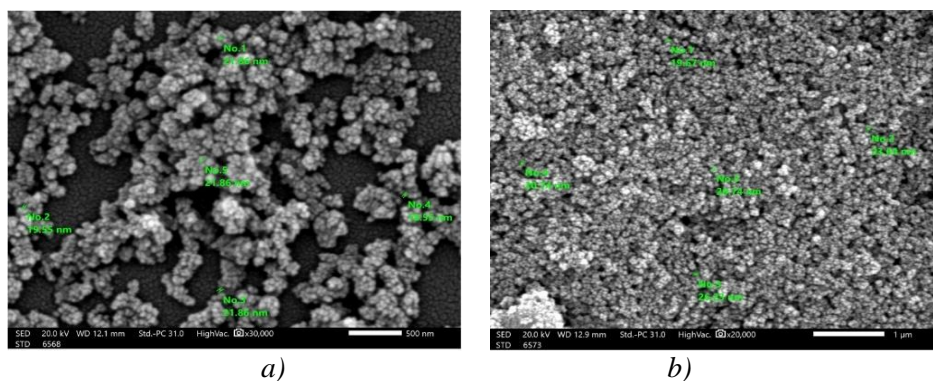


Fig. 1. SEM image of (a) ZnO nanoparticles and (b) ZnO/ MnPcCl NP composite.

The TEM has been recently used to diagnose different types of materials [30]. TEM technique explains the compositional, topographical, and morphological characterizations of solid materials. Furthermore, it provides information about particle size and microstructures information [31]. Figure 2 (a-c) shows a TEM image of ZnO nanoparticles at different scales 50, 100, and 200 nm, respectively, while Figure 1d depicts a selected area electron diffraction (SAED). The images in Figure 1 confirm the ZnO particles distributed homogeneously in spherical shape in an average size of 18-20 nm. Figure 2(a-d) assures that ZnO has a high crystalline shape and high porous nanostructure. The encapsulation efficiency (EE) of MnPcCl was 92.30% and the load capacity (LC) was 9.23 %.



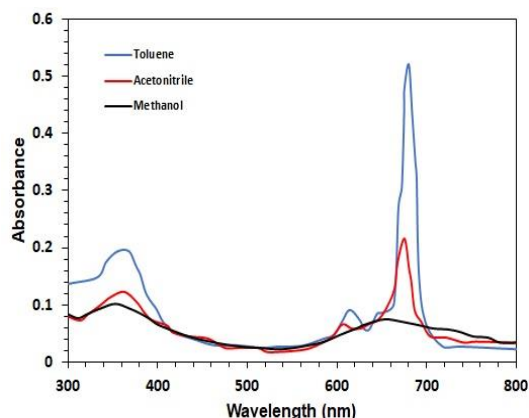


Fig. 4. Absorbance spectrum of ZnO/MnPcCl NPs.

As shown in Figure 5, the ROS percentage of the level of oxidant species generated by ZnO/MnPcCl NPs in PBS was equivalent to more than 60% of that observed with free MPC in ethanol under irradiation with a laser ( $\lambda$  670 nm;  $0.6 \text{ J/cm}^2$  energy density). Generation of reactive oxygen ZnO/MnPcCl NPs was higher than free MnPcCl in PBS under the same irradiation conditions. This finding indicates that the encapsulation of MnPcCl in ZnO NPs enhances the photochemical performance of MnPcCl in aqueous media. These results are in accordance with the previous studies on the different formulas of Phthalocyanines [34-36].

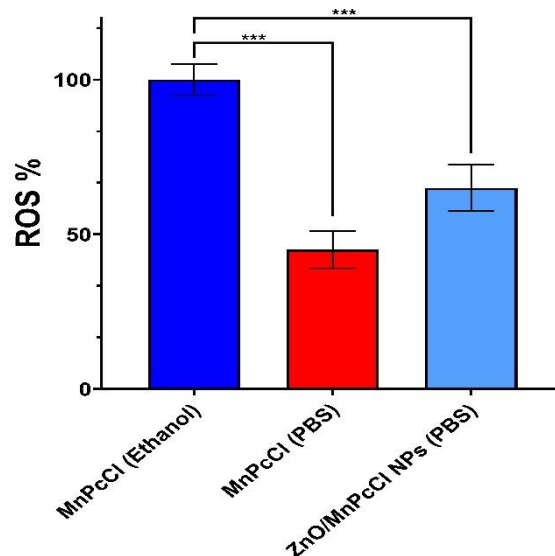


Fig. 5. Generation of reactive oxygen species for free MnPcCl NPs ( $1 \mu\text{M}$ ) in ethanol, free MnPcCl NPs ( $1 \mu\text{M}$ ) PBS, and dissolved ZnO/MnN3-PcinCl NPs in PBS under irradiation with a laser ( $\lambda$  670 nm;  $0.6 \text{ J/cm}^2$  energy density).

NPs could be administered by intravenous injection; hence hemocompatibility is one of the most important tests that should be done to evaluate the cytotoxicity of nanoparticles [37, 38]. Hemolysis and blood coagulation tests are approved to be used to assess the hemocompatibility of NPs in vitro [39-41]. Figure 6 shows the hemolysis percentage due to the incubation of blood with ZnO/MnPcCl NPs. The percentages of hemolysis due to incubation with ZnO/MnPcCl NPs with and without irradiation were below 2%, confirming their hemocompatibility. The hemolysis caused by ZnO/MnPcCl NPs ( $1.6 \pm 0.1\%$ ) was significantly higher than that observed in the control ( $p < 0.05$ ). The percent hemolysis caused by ZnO/MnPcCl NPs incorporated with irradiation by

laser (670 nm;  $0.6 \text{ J/cm}^2$  energy density) was significantly higher than both control and ZnO/MnPcCl NPs in the dark. It was indicated previously that hemolysis is due to NPs depending on the concentration- and surface charge of NPs. Neutral and negatively charged nanoparticles had lower hemolysis compared to positively charged ones [42-44]. The non-hemolytic effect of ZnO/MnPcCl NPs may be due to their natural surface charge.

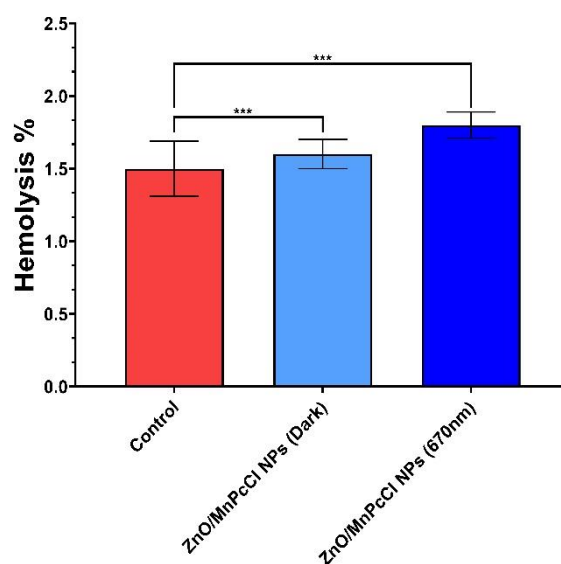


Fig. 6. Hemolytic effect of ZnO/MnPcCl NPs on human blood. \*\*\* Statistically significant difference ( $p < 0.05$ ).

We have evaluated the coagulation effect of ZnO/MnPcCl NPs by measuring prothrombin time (PT) and partial thromboplastin time (PTT), which are frequently used to assess blood clot formation. PT and PTT (Figure 7) for incubation with ZnO/MnPcCl NPs in the dark and under the action of irradiation were in a normal range. There were no significant differences between PT and PTT for plasma incubated with ZnO/MnPcCl NPs and control.

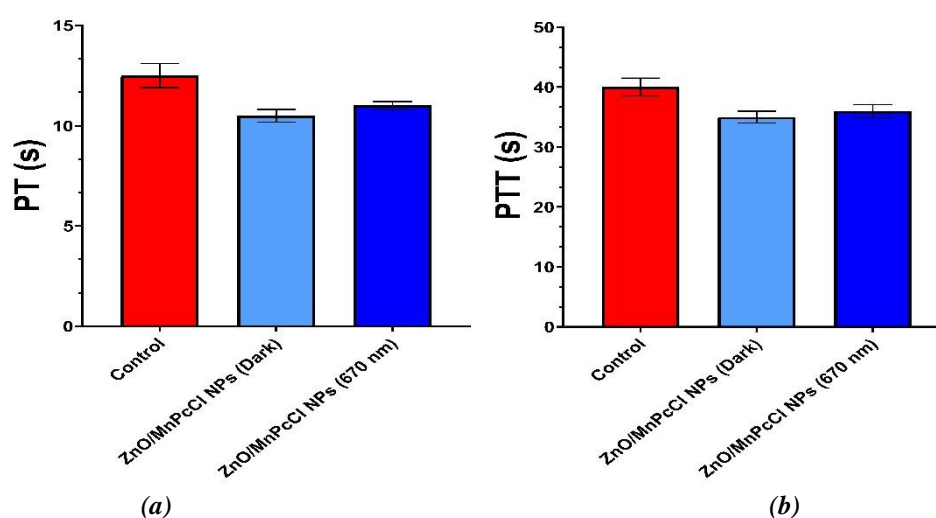


Fig. 7. Coagulation effect of ZnO/MnPcCl NPs on human blood. (a) prothrombin time (b) partial thromboplastin time.

Ehrlich ascites carcinoma implanted in mice was used to evaluate the anticancer effect of ZnO/MnPcCl NPs in vivo. Treatment of all mice groups started before the tumor volume reached

around  $450 \text{ mm}^3$ . Along 15 days, the tumor growth was monitored every three days. Figure 8a shows the changes in the tumor volume over the 15 days of the experiment for different groups. For the group treated with ZnO/MnPcCl NPs in conjunction with laser radiation ( $670 \text{ nm}$ ;  $0.6 \text{ J/cm}^2$ ), a remarkable reduction in tumor volume was indicated. The reduction in tumor volume was gradually in conjunction with treatment during the 15 days.

In contrast, the tumor volume of a control group (untreated) was increased by about 4 folds by the end of 15 days. There was a slight increase in tumor volume between the groups treated with ZnO/MnPcCl NPs and laser, separately, but it did not reach the same level as in the control group. At the end of the experiment, a tumor volume of  $447 \pm 23$  and  $373 \pm 36$ ,  $325 \pm 40$ , and  $123 \pm 15 \text{ mm}^3$  were detected for control, and  $670 \text{ nm}$  radiated group ZnO/MnPcCl NPs treated group, and ZnO/MnPcCl NPs  $670 \text{ nm}$  treated group, respectively. The change in tumor volume of the groups treated with ZnO/MnPcCl NPs and  $670 \text{ nm}$  were highly significant when compared to the control ( $p < 0.05$ ). The tumor volume of the ZnO/MnPcCl NPs /  $670 \text{ nm}$  treated group was much smaller than other groups after 15 days of treatment.

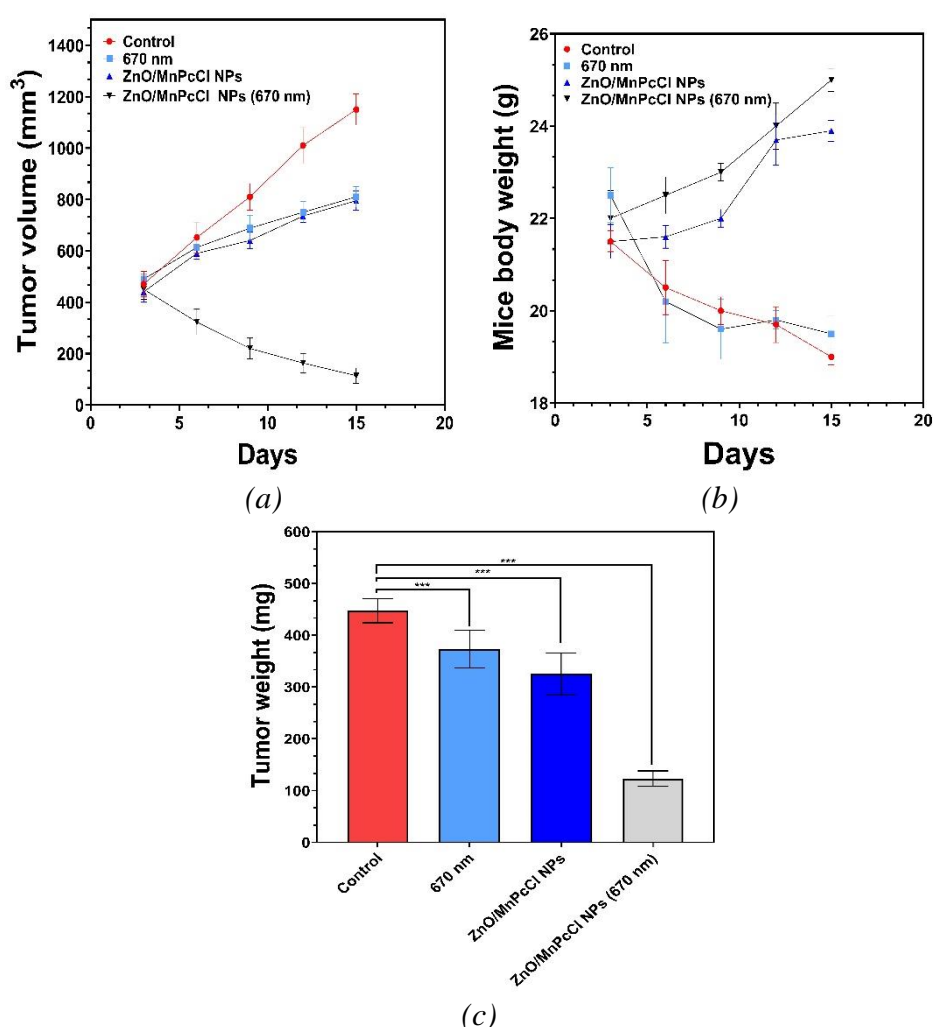


Fig. 8. (a) Ehrlich tumor growth curve (b) Changes in the bodyweight of the Ehrlich tumor-bearing mice as a function of time (c) Weight of the tumor at the end of the study. \*\*\* Statistically significant difference ( $p < 0.05$ ).

In Figure 8b, there is a clear trend of decreasing mice weight between the control group. Following the injection of ZnO/MnPcCl NPs in conjunction with laser radiation, a significant increase ( $p < 0.05$ ) in mice weight was recorded. At the end of 15 days, the mice were sacrificed, and the tumors were removed and weighed. It is apparent from Figure 8c that the tumor weight in

the ZnO/MnPcCl NPs 670 nm group was significantly much smaller than that of other groups ( $p < 0.05$ ). These findings agree with the previous studies that showed Pc and its derivatives could be used effectively as anti-cancer therapy [14, 45].

#### 4. Conclusion

ZnO/MnPcCl NPs were prepared using a simple and efficient procedure. The prepared NPs were highly hemocompatible. Further, the ZnO/MnPcCl NPs in association with laser had significantly higher cytotoxic effects on Ehrlich tumor-bearing mice when compared with laser only. These findings confirm that ZnO/MnPcCl NPs could establish a nanocarrier system for PDT with a good potential to enhance anticancer properties. The present study provides additional evidence that the application of nanotechnology to PDT could enhance cancer therapy. In addition, this could reduce the cytotoxicity of the Ps and increase stability and delivery efficiency.

#### Acknowledgments

The authors extend their appreciation to the Deanship of Scientific Research at University of Tabuk for funding this work through Research Group RGP-S-1441-008.

#### References

- [1] Bergh, J., Quo vadis with targeted drugs in the 21st century? 2009, American Society of Clinical Oncology. <https://doi.org/10.1200/JCO.2008.18.8342>
- [2] Agostinis, P., et al., Photodynamic therapy of cancer: an update. CA: a cancer journal for clinicians, 2011. 61(4): p. 250-281 <https://doi.org/10.3322/caac.20114>
- [3] Falk- Mahapatra, R. and S.O. Gollnick, Photodynamic therapy and immunity: an update. Photochemistry and photobiology, 2020. 96(3): p. 550-559. <https://doi.org/10.1111/php.13253>
- [4] Henderson, B.W., Photodynamic therapy: basic principles and clinical applications. 2020: CRC Press. <https://doi.org/10.1201/9781003066897>
- [5] Pushpan, S., et al., Porphyrins in photodynamic therapy-a search for ideal photosensitizers. Current Medicinal Chemistry-Anti-Cancer Agents, 2002. 2(2): p. 187-207. <https://doi.org/10.2174/1568011023354137>
- [6] Zhang, J., et al., An updated overview on the development of new photosensitizers for anticancer photodynamic therapy. Acta pharmaceutica sinica B, 2018. 8(2): p. 137-146 <https://doi.org/10.1016/j.apsb.2017.09.003>
- [7] Kwiatkowski, S., et al., Photodynamic therapy-mechanisms, photosensitizers and combinations. Biomedicine & pharmacotherapy, 2018. 106: p. 1098-1107 <https://doi.org/10.1016/j.biopha.2018.07.049>
- [8] Perotti, C., et al., Porphyrin synthesis from ALA derivatives for photodynamic therapy. In vitro and in vivo studies. British journal of cancer, 2004. 90(8): p. 1660-1665. <https://doi.org/10.1038/sj.bjc.6601722>
- [9] Patrice, T., Photodynamic therapy. Vol. 2. 2003: Royal Society of Chemistry. <https://doi.org/10.1039/9781847551658>
- [10] Lange, C. and P. J Bednarski, Photosensitizers for photodynamic therapy: Photochemistry in the service of oncology. Current pharmaceutical design, 2016. 22(46): p. 6956-6974 <https://doi.org/10.2174/1381612822666161124155344>
- [11] Lomax, S.Q., Phthalocyanine and quinacridone pigments: their history, properties and use. Studies in Conservation, 2005. 50(sup1): p. 19-29 <https://doi.org/10.1179/sic.2005.50.Supplement-1.19>
- [12] Miller, J.D., et al., Photodynamic therapy with the phthalocyanine photosensitizer Pc 4: the case experience with preclinical mechanistic and early clinical-translational studies. Toxicology

and applied pharmacology, 2007. 224(3): p. 290-299

<https://doi.org/10.1016/j.taap.2007.01.025>

[13] Yan, S., et al., Effects of hydroxyl radicals produced by a zinc phthalocyanine photosensitizer on tumor DNA. *Dyes and Pigments*, 2020. 173: p. 107894

<https://doi.org/10.1016/j.dyepig.2019.107894>

[14] Zheng, B.-Y., et al., Phthalocyanine-based photosensitizers combined with anti-PD-L1 for highly efficient photodynamic immunotherapy. *Dyes and Pigments*, 2021. 185: p. 108907

<https://doi.org/10.1016/j.dyepig.2020.108907>

[15] Lever, A.P., The phthalocyanines. *Advances in Inorganic Chemistry and Radiochemistry*, 1965. 7: p. 27-114 [https://doi.org/10.1016/S0065-2792\(08\)60314-3](https://doi.org/10.1016/S0065-2792(08)60314-3)

[16] Durmuş, M., V. Ahsen, and T. Nyokong, Photophysical and photochemical studies of long chain-substituted zinc phthalocyanines. *Journal of Photochemistry and Photobiology A: Chemistry*, 2007. 186(2-3): p. 323-329. <https://doi.org/10.1016/j.jphotochem.2006.08.025>

[17] Lever, A.B.P. and C.C. Leznoff, *Phthalocyanines: properties and applications*. 1996: New York: VCH, 1989-c1996.

[18] Allen, C.M., W.M. Sharman, and J.E. Van Lier, Current status of phthalocyanines in the photodynamic therapy of cancer. *Journal of Porphyrins and Phthalocyanines*, 2001. 5(02): p. 161-169 <https://doi.org/10.1002/jpp.324>

[19] Calixto, G.M.F., et al., Nanotechnology-based drug delivery systems for photodynamic therapy of cancer: a review. *Molecules*, 2016. 21(3): p. 342

<https://doi.org/10.3390/molecules21030342>

[20] Zheng, Y., et al., Nanoparticle-based drug delivery systems for controllable photodynamic cancer therapy. *European Journal of Pharmaceutical Sciences*, 2020. 144: p. 105213

<https://doi.org/10.1016/j.ejps.2020.105213>

[21] Chilakamarthi, U. and L. Giribabu, Photodynamic therapy: past, present and future. *The Chemical Record*, 2017. 17(8): p. 775-802. <https://doi.org/10.1002/tcr.201600121>

[22] Dąbrowski, J.M., et al., Engineering of relevant photodynamic processes through structural modifications of metallotetrapyrrolic photosensitizers. *Coordination Chemistry Reviews*, 2016. 325: p. 67-101. <https://doi.org/10.1016/j.ccr.2016.06.007>

[23] Trindade, A.C., et al., Gelatin nanoparticles via template polymerization for drug delivery system to photoprocess application in cells. *Journal of Biomaterials Science, Polymer Edition*, 2021(just-accepted): p. 1-14. <https://doi.org/10.1080/09205063.2021.1998819>

[24] Gill, K.K., A. Kaddoumi, and S. Nazzal, PEG-lipid micelles as drug carriers: physiochemical attributes, formulation principles and biological implication. *Journal of drug targeting*, 2015. 23(3): p. 222-231. <https://doi.org/10.3109/1061186X.2014.997735>

[25] Mironov, A.F., K.A. Zhdanova, and A.B. Natal'ya, Nanosized vehicles for delivery of photosensitizers in photodynamic diagnosis and therapy of cancer. *Russian Chemical Reviews*, 2018. 87(9): p. 859. <https://doi.org/10.1070/RCR4811>

[26] Muehlmann, L.A., et al., Aluminium-phthalocyanine chloride nanoemulsions for anticancer photodynamic therapy: Development and in vitro activity against monolayers and spheroids of human mammary adenocarcinoma MCF-7 cells. *Journal of nanobiotechnology*, 2015. 13(1): p. 1-11. <https://doi.org/10.1186/s12951-015-0095-3>

[27] He, X., et al., Methylene blue-encapsulated phosphonate-terminated silica nanoparticles for simultaneous in vivo imaging and photodynamic therapy. *Biomaterials*, 2009. 30(29): p. 5601-5609. <https://doi.org/10.1016/j.biomaterials.2009.06.030>

[28] Spiller, W., et al., *Singlet oxygen quantum yields of different photosensitizers in polar solvents and micellar solutions*. *Journal of Porphyrins and Phthalocyanines*, 2012.

[29] Anucha, C.B., et al., Synthesis, characterization, and photocatalytic evaluation of manganese (III) phthalocyanine sensitized ZnWO<sub>4</sub> (ZnWO<sub>4</sub>MnPc) for bisphenol a degradation under UV irradiation. *Nanomaterials*, 2020. 10(11): p. 2139. <https://doi.org/10.3390/nano10112139>

[30] Fultz, B. and J.M. Howe, *Transmission electron microscopy and diffractometry of materials*. 2012: Springer Science & Business Media.

[31] Darwish, A., et al., Thin films of nanostructured gallium (III) chloride phthalocyanine deposited on FTO: Structural characterization, optical properties, and laser optical limiting. *Physica B: Condensed Matter*, 2020. 593: p. 412321. <https://doi.org/10.1016/j.physb.2020.412321>

- [32] Seoudi, R., G. El-Bahy, and Z. El Sayed, FTIR, TGA and DC electrical conductivity studies of phthalocyanine and its complexes. *Journal of Molecular Structure*, 2005. 753(1-3): p. 119-126 <https://doi.org/10.1016/j.molstruc.2005.06.003>
- [33] Janaki, A.C., E. Sailatha, and S. Gunasekaran, Synthesis, characteristics and antimicrobial activity of ZnO nanoparticles. *Spectrochimica Acta Part A: Molecular and Biomolecular Spectroscopy*, 2015. 144: p. 17-22. <https://doi.org/10.1016/j.saa.2015.02.041>
- [34] Muehlmann, L.A., et al., Aluminum-phthalocyanine chloride associated to poly (methyl vinyl ether-co-maleic anhydride) nanoparticles as a new third-generation photosensitizer for anticancer photodynamic therapy. *International journal of nanomedicine*, 2014. 9: p. 1199 <https://doi.org/10.2147/IJN.S57420>
- [35] Lovell, J.F., et al., Activatable photosensitizers for imaging and therapy. *Chemical reviews*, 2010. 110(5): p. 2839-2857. <https://doi.org/10.1021/cr900236h>
- [36] Master, A.M., et al., Delivery of the photosensitizer Pc 4 in PEG-PCL micelles for in vitro PDT studies. *Journal of pharmaceutical sciences*, 2010. 99(5): p. 2386-2398 <https://doi.org/10.1002/jps.22007>
- [37] de la Harpe, K.M., et al., The hemocompatibility of nanoparticles: a review of cell-nanoparticle interactions and hemostasis. *Cells*, 2019. 8(10): p. 1209. <https://doi.org/10.3390/cells8101209>
- [38] Safwat, M.A., et al., Epigallocatechin-3-Gallate-Loaded Gold Nanoparticles: Preparation and Evaluation of Anticancer Efficacy in Ehrlich Tumor-Bearing Mice. *Pharmaceuticals*, 2020. 13(9): p. 254. <https://doi.org/10.3390/ph13090254>
- [39] Williams, D.F., On the mechanisms of biocompatibility. *Biomaterials*, 2008. 29(20): p. 2941-2953. <https://doi.org/10.1016/j.biomaterials.2008.04.023>
- [40] Dobrovolskaia, M.A., et al., Method for analysis of nanoparticle hemolytic properties in vitro. *Nano letters*, 2008. 8(8): p. 2180-2187. <https://doi.org/10.1021/nl0805615>
- [41] Love, S.A., J.W. Thompson, and C.L. Haynes, Development of screening assays for nanoparticle toxicity assessment in human blood: preliminary studies with charged Au nanoparticles. *Nanomedicine*, 2012. 7(9): p. 1355-1364. <https://doi.org/10.2217/nnm.12.17>
- [42] S Singh, N., S.K. Sahoo, and R. Kumar, Hemolysis tendency of anticancer nanoparticles changes with type of blood group antigen: An insight into blood nanoparticle interactions. *Materials Science and Engineering: C*, 2020. 109: p. 110645 <https://doi.org/10.1016/j.msec.2020.110645>
- [43] Neun, B.W., A.N. Ilinskaya, and M.A. Dobrovolskaia, Updated method for in vitro analysis of nanoparticle hemolytic properties, in *Characterization of nanoparticles intended for drug delivery*. 2018, Springer. p. 91-102. [https://doi.org/10.1007/978-1-4939-7352-1\\_9](https://doi.org/10.1007/978-1-4939-7352-1_9)
- [44] Babu, E.P., et al., Size dependent uptake and hemolytic effect of zinc oxide nanoparticles on erythrocytes and biomedical potential of ZnO-ferulic acid conjugates. *Scientific reports*, 2017. 7(1): p. 1-12. <https://doi.org/10.1038/s41598-017-04440-y>
- [45] Ozdemir, M., et al., Phthalocyanines bearing silazane group for colorectal cancer. *Dyes and Pigments*, 2021. 196: p. 109832. <https://doi.org/10.1016/j.dyepig.2021.109832>